



An effective classification and numbering system for dental bitewing radiographs using teeth region and contour information

P.L. Lin^a, Y.H. Lai^b, P.W. Huang^{b,*}

^a Department of Computer Science and Information Engineering, Providence University, Shalu, Taichung 43301, Taiwan

^b Department of Computer Science and Engineering, National Chung Hsing University, Taichung 40227, Taiwan

ARTICLE INFO

Article history:

Received 12 December 2008

Received in revised form

4 September 2009

Accepted 10 October 2009

Keywords:

Dental bitewing radiograph

Homomorphic filter

Homogeneity measurement

Adaptive contrast stretching

Teeth classification

Sequence alignment

Teeth numbering

ABSTRACT

We propose a dental classification and numbering system to effectively segment, classify, and number teeth in dental bitewing radiographs. An image enhancement method that combines homomorphic filtering, homogeneity-based contrast stretching, and adaptive morphological transformation is proposed to improve both contrast and illumination evenness of the radiographs simultaneously. Iterative thresholding and integral projection are adapted to isolate teeth to regions of interest (ROIs) followed by contour extraction of the tooth and the pulp (if available) from each ROI. A binary linear support vector machine using the skew-adjusted relative length/width ratios of both teeth and pulps, and crown size as features is proposed to classify each tooth to molar or premolar. Finally, a numbering scheme that combines a missing teeth detection algorithm and a simplified version of sequence alignment commonly used in bioinformatics is presented to assign each tooth a proper number. Experimental results show that our system has accuracy rates of 95.1% and 98.0% for classification and numbering, respectively, in terms of number of teeth tested, and correctly classifies and numbers the teeth in four images that were reported either misclassified or erroneously numbered, respectively.

© 2009 Elsevier Ltd. All rights reserved.

1. Introduction

Biometric recognition systems based on physiological and behavioral characteristics such as face, voice, and iris can provide reliable identification in many applications. However, most of these characteristics are not suitable for postmortem identification in law enforcement, especially under the severe decaying of soft tissues or mass disasters such as fire or collision [1]. Teeth, being the hardest and the most impregnable part of human body, are thus regarded to be the best candidates for postmortem identification. For automatic and accurate identification, Automatic Dental Identification System (ADIS) [2], which involves teeth segmentation, teeth classification, teeth numbering, and human identification, has been proposed and investigated.

The adult dentition contains 32 teeth, 16 in each of the upper jaw (maxilla) and the lower jaw (mandible), respectively. Based on the Universal numbering system as shown in Fig. 1 [3], numbers 1, 2, and 3 are the third, the second, and the first molar whereas numbers 4 and 5 are the second and the first premolar of the right maxilla, respectively. Number 6 is the canine tooth. Following around the upper arch to the left, numbers 11–16 are the canine,

the first and the second premolars, and the first to the third molars of the left maxilla, respectively. Descending to the lower jaw, numbers 17–22 and 32–27 are the third to the first molars, the second and the first premolars, and canine of the left and the right mandible, respectively. Fig. 2 shows four bitewing radiographs, where (a) and (b) are taken from the right side, and (c) and (d) are taken from the left side. Generally, four components exist in a bitewing dental radiograph: teeth, pulps, gums, and air/background, as shown in Fig. 3. The isolated blocks that each contains a single tooth are usually called regions of interest (ROIs). Within each tooth, the upper portion bounded by the center of the pulp is called the crown part, and the lower portion is called the root part.

Several good progresses have been made for teeth segmentation in the past few years. Jain and Chen [4] proposed a semi-automatic contour extraction method for tooth segmentation by using integral projection and Bayes rule, in which an initial valley gap point is required for applying the integral projection to tooth isolation. Zhou and Abdel-Mottaleb [5] presented a segmentation method that consists of image enhancement, ROI localization, and tooth segmentation by using morphological operations and Snake method. Nomir and Abdel-Mottaleb [6] developed a fully automated approach based on iterative thresholding and adaptive thresholding for segmentation. Keshtkar and Gueaieb [7] introduced a swarm-intelligence-based and a cellular-automata model approach. Said et al. [8] offered a mathematical morphology

* Corresponding author. Tel.: +886 4 2285 1528; fax: +886 4 2285 3870.

E-mail addresses: lan@pu.edu.tw (P.L. Lin), yanhao.lai@gmail.com (Y.H. Lai), powhei.huang@msa.hinet.net (P.W. Huang).

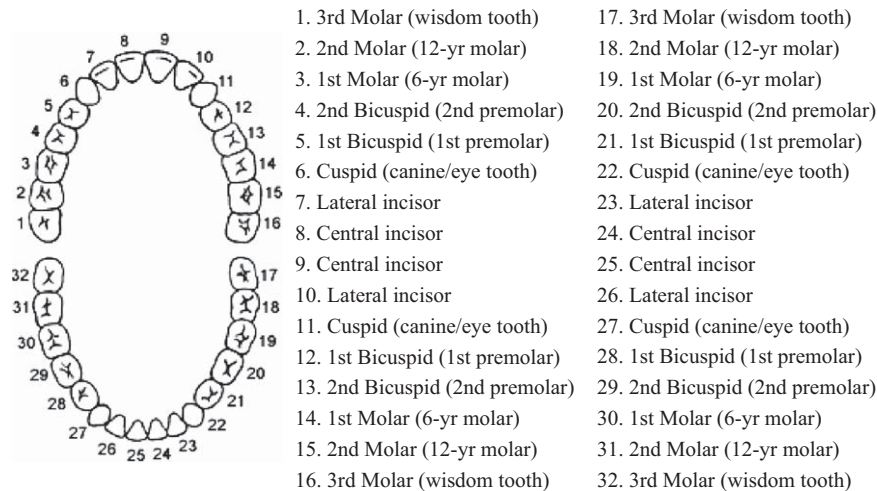


Fig. 1. The universal numbering system.

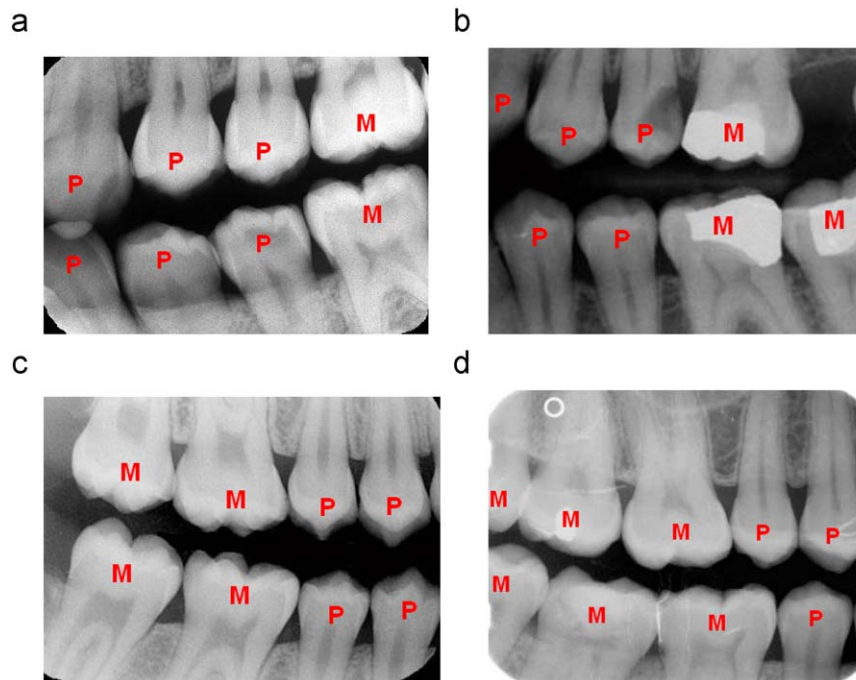


Fig. 2. Bitewing radiographs. (a) and (b) are taken from the left side, (c) and (d) are taken from the right side.

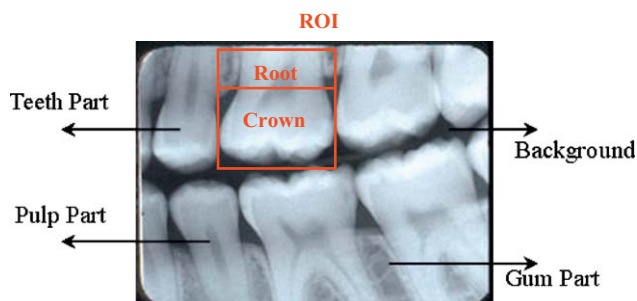


Fig. 3. Different portions in a bitewing radiograph.

approach, which used a series of morphology filtering operations to improve the segmentation, and then analyzed the connected components to obtain the desired ROIs. Li et al. [9] proposed a

semi-automatic lesion detection framework by using two coupled level set functions in which initial contour are derived from a trained support vector machine (SVM) to detect areas of lesions from dental X-ray images. All of these methods directly use greyscale intensity for segmentation. However, only considering greyscale intensity tends to fail images with fuzzy teeth contours and low-contrast between teeth and gums. We proposed a segmentation method using texture-based features and fuzzy rule-based region growing [10] to reduce the effects of both problems. Although good results had been obtained for many images, the method did not perform well for radiographs with uneven exposure and unobvious texture in gums.

In traditional identification, each tooth in the query image needs to be compared with all teeth stored in the database, which is tedious and time consuming. Teeth classification and numbering can identify each tooth as the specific one in the universal teeth numbering system [3]. This approach will limit the search

space to only including the teeth with the same assigned number and consequently improves the identification accuracy. The shape of the teeth has been proposed as a piece of useful information for classification in literature. In general, there are two types of shape representations, i.e., contour-based and region-based, and each type has various methods with varying performance for different shapes. Methods with region-based representation, such as moments invariants [11], tend to work well on objects where the distribution of the pixels is informative; whereas methods with contour-based representation, such as Fourier descriptors of the boundaries used in [12], can work better on objects where their outline carries more information. These methods, however, did not result in high classification accuracy, especially for those poorly skewed radiographs in those teeth at one side are nearly half appeared.

For numbering techniques, Mahoor and Abdel-Mottaleb [12] proposed a method that checks to which in the set of various-length standard patterns the classified teeth arrangement matches and assigns a number to each tooth when a match occurs. The major limitation of their method is that it does not consider the case of missing teeth, nor can it assign teeth numbers when no pattern matches exactly. Jain and Chen [13] proposed a registration method that uses a hidden Markov model (HMM) as an underlying representation of the dental atlas to handle the problem of missing teeth. In their model, the states representing the available teeth have class of each tooth, whereas the states representing missing teeth have the distance between neighbouring teeth. Although the method had been demonstrated promising for most periapical images, errors still occurred when too few

correctly classified teeth in the teeth sequence or when missing teeth not been correctly detected, which are often the classification results of skewed bitewing images.

In this paper, we propose a dental classification and numbering system to effectively classify and number teeth in dental bitewing radiographs. As shown in Fig. 4, our system includes an image enhancement method that combines the homomorphic filtering technique to reduce uneven exposure problem and adaptive contrast stretching based on homogeneity of both texture and intensity to improve low-contrast problem. For solving problems of incomplete view of some teeth, we propose ROI extension with angle adjustment so that closer to valid length/width ratios of teeth can be obtained for classification. We also propose using relative crown sizes and length/width ratios of pulps besides teeth as three features for teeth classification with SVM. Finally, we propose a numbering algorithm, which combines a missing teeth detection algorithm and a simplified sequence alignment commonly used in bioinformatics, to align the teeth sequence of each jaw to the best matching segment within one of the standard pattern and assign a proper number to each tooth.

The remainder of this paper is organized as follows. In Section 2, the segmentation method that includes our proposed image enhancement, the adapted teeth segmentation, the isolation, and contour extraction is described. In Section 3, the proposed ROI extension with angle adjustment, the classifier, and three features used are explained. A missing teeth detection method and a modified sequence alignment algorithm for teeth numbering are described in Section 4. Experimental results and comparisons to

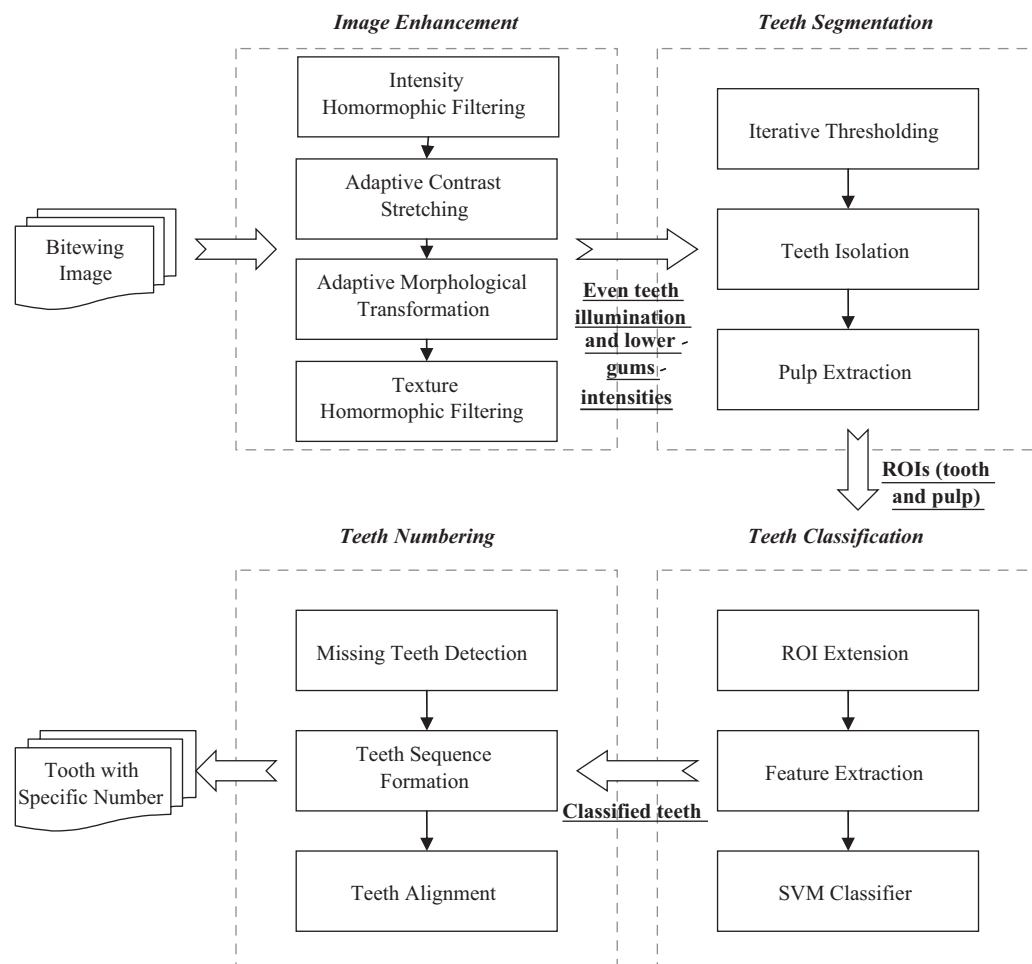


Fig. 4. The block diagram of our system.

demonstrate the effectiveness of our method are provided in Section 5. Finally, the conclusions are given in Section 6.

2. Teeth segmentation

Based on our observation on the available dental bitewing images, the shapes of teeth and pulps play important roles in accurate classification. Thus, accurate segmentation to teeth and pulps can improve teeth classification and facilitate correct teeth numbering.

2.1. Image enhancement

Dental radiographs always suffer from problems like noise, low-contrast, and uneven exposure, as shown in Figs. 5(a) and (b). These problems are either handled by adaptive intensity stretching and top- and bottom-hat morphological transformations [8] or by adaptive thresholding and top- and bottom-hat morphological transformations [12]. However, the contrast between teeth and pulps and uneven intensity of teeth across the entire radiograph cannot be simultaneously taken care by either method. In order to improve both contrast and intensity evenness simultaneously, we propose an image enhancement method that combines homomorphic filtering, adaptive contrast stretching based on homogeneity [10], and adaptive morphological transformations.

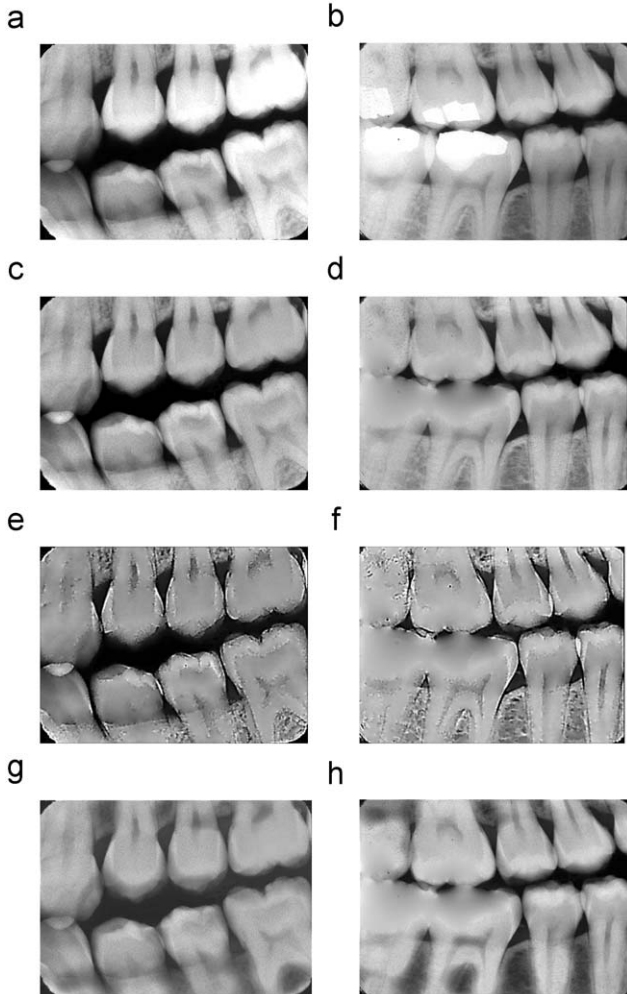


Fig. 5. Image enhancement: (a), (b) original images, (c), (d) images after the first homomorphic filtering, (e), (f) after adaptive contrast stretching and morphological transformations, (g), (h) final enhanced images.

2.1.1. Homomorphic filtering

Homomorphic filters are widely used in image processing for compensating the effect of non-uniform illumination in an image [14]. In theory, an image function $I(x,y)$ may be characterized by the multiplicative combination of an illumination component $i(x,y)$ and a reflectance component $r(x,y)$.

$$I(x,y) = i(x,y) \cdot r(x,y). \quad (1)$$

Also, teeth, pulps, and gums in a dental radiograph should each have similar reflectivity. Thus, we propose a homomorphic filtering method to suppress the uneven illumination effect while preserving the intensity discrepancies among all the components in the radiograph.

Proposed homomorphic filter: For a given dental radiograph image $I(x,y)$, we first take the Fourier transform of the logarithm of $I(x,y)$ to get the sum of its low-frequency illumination component and high-frequency reflectance component.

$$\mathbf{I}(u,v) = \mathcal{F}(\ln(I(x,y))) = \mathcal{F}(\ln(i(x,y))) + \mathcal{F}(\ln(r(x,y))). \quad (2)$$

We then apply a Gaussian low-pass filter $\mathcal{G}(u,v)$ [15] to \mathbf{I} to remove its detailed components and retain its illumination distribution:

$$\mathbf{I}'(u,v) = \mathcal{G}(u,v) \cdot \mathbf{I}(u,v). \quad (3)$$

$$\mathcal{G}(u,v) = \frac{1}{\sqrt{2\pi}\sigma} e^{-(u^2+v^2)/2\sigma^2}. \quad (4)$$

As the rims of teeth have been removed during Gaussian filtering, we want to restore the rims back using a spatial dilation function. So we invert-transform \mathbf{I}' back to spatial domain and take antilogarithm to obtain a filtered homomorphic view of illumination.

$$I'(x,y) = \ln^{-1} \mathcal{F}^{-1}(\mathbf{I}'(u,v)). \quad (5)$$

We then apply a dilation \mathcal{D} to include back the filtered rims of teeth as much as possible. Finally we remove the illumination effect from the original image by dividing it with the dilated homomorphic view of illumination to result in a homomorphic filtered image I^* that will appear much more uniformly illuminated.

$$I^*(x,y) = \frac{I(x,y)}{\mathcal{D}(I'(x,y))} = i^*(x,y) \cdot r^*(x,y). \quad (6)$$

where $i^*(x,y)$ and $r^*(x,y)$ represent the homomorphic filtered illumination and reflectance components, respectively.

Eqs. (5) and (6) are equivalent to transform the spatially dilated image back to frequency domain again without taking anti-logarithm then subtract it from \mathbf{I} and take the inverse Fourier transform and anti-logarithm to it. That is,

$$\mathbf{I}^*(u,v) = \mathcal{F}(\mathcal{D}(\mathcal{F}^{-1}(\mathbf{I}'(u,v)))) = \mathcal{F}(\ln(i'(x,y))) + \mathcal{F}(\ln(r'(x,y))). \quad (7)$$

$$I^*(x,y) = \ln^{-1} \mathcal{F}^{-1}(\mathbf{I}^*(u,v)) = i^*(x,y) \cdot r^*(x,y). \quad (8)$$

where $i'(x,y)$ and $r'(x,y)$ represent the dilated-Gaussian filtered illumination and reflectance components, respectively.

2.1.2. Adaptive contrast stretching based on homogeneity

Homogeneity is a mathematic statistic measurement that reflects the degree of uniformity in a region of interest [16]. In our previous work [10], we presented an adaptive contrast stretching technique based on a homogeneity measurement $H(x,y)$, which is defined as a combination of the complement of three normalized local discrepancy measurements: local range value, local standard deviation, and impulsiveness of the distribution. Local range value, denoted $d(x,y)$, measures the difference between the maximum and the minimum value of the neighborhood pixels within a window $\mathcal{W}(x,y)$ that is centered

at (x,y) with both of its width and length equal to w , respectively. Local standard deviation, denoted $v(x,y)$, and $\gamma_4(x,y)$ measure the dispersion and the impulsiveness within a neighborhood $\mathcal{W}(x,y)$, respectively. The mathematic expressions of our homogeneity definition are as follows.

$$H(x,y) = (1 - D(x,y)) \cdot (1 - V(x,y)) \cdot (1 - R_4(x,y)). \quad (9)$$

$$D(x,y) = \frac{d(x,y)}{\max_{\Omega}\{d(x,y)\}}, V(x,y) = \frac{v(x,y)}{\max_{\Omega}\{v(x,y)\}}, \quad (10)$$

$$R_4(x,y) = \frac{\gamma_4(x,y)}{\max_{\Omega}\{\gamma_4(x,y)\}}.$$

$$d(x,y) = \max\{I(x+p,y+q) - \min\{I(x+p,y+q)\}, \text{ where } -\lfloor w/2 \rfloor \leq p, q \leq \lfloor w/2 \rfloor\}, \quad (11)$$

$$v(x,y) = \sqrt{\frac{1}{w^2} \sum_{p=-\lfloor w/2 \rfloor}^{\lfloor w/2 \rfloor} \sum_{q=-\lfloor w/2 \rfloor}^{\lfloor w/2 \rfloor} I(x+p,y+q) - \mu(x,y)^2}. \quad (12)$$

$$\gamma_4(x,y) = \frac{\sum_{p=-\lfloor w/2 \rfloor}^{\lfloor w/2 \rfloor} \sum_{q=-\lfloor w/2 \rfloor}^{\lfloor w/2 \rfloor} I(x+p,y+q) - \mu(x,y)^4}{w^2 - 1}. \quad (13)$$

and

$$\mu(x,y) = \frac{1}{w^2} \sum_{p=-\lfloor w/2 \rfloor}^{\lfloor w/2 \rfloor} \sum_{q=-\lfloor w/2 \rfloor}^{\lfloor w/2 \rfloor} I(x+p,y+q). \quad (14)$$

where Ω is the domain of I , I is a scalar intensity map, and $\lfloor w/2 \rfloor$ stands for the largest integer smaller than $w/2$.

Based on the definition, a region is considered perfectly uniform when $D(x,y)$, $V(x,y)$, and $R_4(x,y)$ in the region are all 0, and the more uniform a region is, the larger the homogeneity measurement of the pixels within it will be. The adaptive contrast stretching function is constructed as follows.

- (1) Calculate the degree of non-homogeneity $NH(x,y)$ for each pixel (x,y) by

$$NH(x,y) = 1 - H(x,y) \quad (15)$$

- (2) Compute the control point “ m ” of the stretching function, which is the mean non-homogeneity $\delta(x,y)$ for window

$\mathcal{W}(x,y)$ centered at pixel (x,y)

$$\delta(x,y) = \frac{\sum_{p=-\lfloor w/2 \rfloor}^{\lfloor w/2 \rfloor} \sum_{q=-\lfloor w/2 \rfloor}^{\lfloor w/2 \rfloor} I(x+p,y+q) \cdot NH(x+p,y+q)}{\sum_{p=-\lfloor w/2 \rfloor}^{\lfloor w/2 \rfloor} \sum_{q=-\lfloor w/2 \rfloor}^{\lfloor w/2 \rfloor} NH(x+p,y+q)}. \quad (16)$$

- (3) Extend the range of NH from $[0,1]$ to $[-1,1]$ by $NH = 2NH - 1$ so that the value becomes negative when the point is within a smooth region and vice versa.

- (4) Determine the other control points “ a ”, “ b ”, and slope “ h ” as $h = v(x,y) \cdot NH(x,y) \cdot C$.

$$\begin{cases} a_x = \delta(x,y) - v(x,y) \\ b_x = \delta(x,y) + v(x,y) \end{cases} \quad \begin{cases} a_y = a_x - h \\ b_y = b_x + h \end{cases} \quad (18)$$

where a_x , a_y , b_x , and b_y denote the coordinates of control points “ a ” and “ b ”, respectively, and the parameter C is a magnification constant. Fig. 6 depicts the concept of the adaptive local contrast stretching function.

Note that the range of $NH(x,y)$ in Eq. (17) is extended to $[-1,1]$ from $[0,1]$. The region is smooth when the value is negative, and the larger the absolute value is, the more uniform the region (i.e. teeth part) will be. On the other hand, positive value means lots of textures exist in the region (i.e. gums). Thus, a smooth function and a sharp function are constructed for teeth and gums, respectively.

- (5) Map every pixel value $I(x,y)$ to a new value $I_c(x,y)$ according to the adaptive stretching function as follows:

$$I_c(x,y) = \begin{cases} (a_y/a_x) \cdot I(x,y), & \text{if } I(x,y) \leq a_x. \\ (b_y - a_y)/(b_x - a_x) \cdot (I(x,y) - a_x) + a_y, & \text{if } a_x < I(x,y) < b_x. \\ (255 - b_y)/(255 - b_x) \cdot (I(x,y) - b_x) + b_y, & \text{if } I(x,y) \geq b_x. \end{cases} \quad (19)$$

2.1.3. Adaptive morphological transformation

After applying the adaptive local contrast stretching, the teeth become smoother, and the gums become more textured. For accentuating the cobweb-like texture, which has small bright and dark spots, without influencing the smooth region, we propose using an adaptive morphological transformation, which is defined as the combination of morphological top-hat and bottom-hat

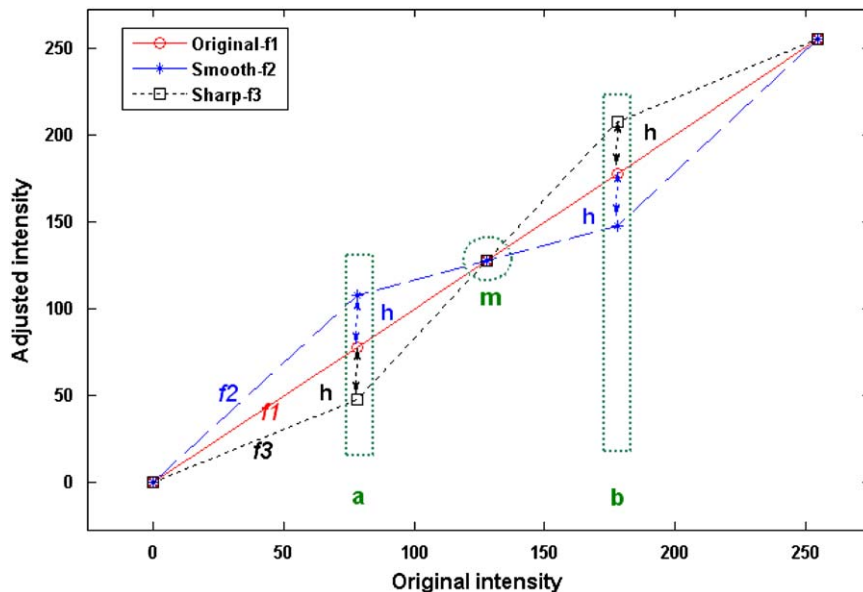


Fig. 6. A concept of adaptive local contrast stretching function.

transformations [17], to further emphasize the texture in the gums.

$$I_E(x, y) = I_c(x, y) + (T(x, y) - B(x, y)) \cdot NH(x, y), \quad (20)$$

where

$$T(x, y) = I(x, y) - (I(x, y) \circ S)$$

$$B(x, y) = (I(x, y) \bullet S) - I(x, y),$$

The operators \circ and \bullet represent morphological opening and closing used in top-hat transformation T and bottom-hat transformation B with a disk structure element S of radius 3, respectively. Non-homogeneity NH is used for suppressing the influence to smooth regions, e.g., teeth or background, but accentuating the influence to texture regions such as gums.

2.1.4. Image enhancement procedure

The goal of the proposed enhancement method is to make images with the intensity of teeth globally higher than the other parts so that simple iterative thresholding can be adapted for the next step of segmentation. The procedure is as follows.

For a given image I , we first apply the homomorphic filtering to obtain an image with more even intensity across the entire view. Figs. 5(c) and (d) are the filtered results of (a) and (b), respectively. We then apply adaptive contrast stretching based on homogeneity to the filtered image to enlarge texture discrepancies between teeth and gums as well as between teeth and pulps. To accentuate the cobweb-like texture in the gums, which has small bright and dark spots, without influencing the smooth regions, we apply the adaptive morphological transformations and obtain an enhanced image I_E , as shown in Figs. 5(e) and (f).

At this point, the intensity of some gums area may appear too close to teeth. In order to lower the intensity of gums so that gums can be differentiable from teeth by intensity thresholding, we transform I_E to I_F , which is the combination of both entropy and edge value of I_E . Since gums have more texture than teeth even though their average intensity may be close, they have higher entropy and edge value and thus appear brighter than teeth in I_E . That is, gums and edges become the high illumination portion of I_E . So we apply the homomorphic filtering again to remove the high illumination portion and leave gums part appeared darker than teeth. Figs. 5(g) and (h) illustrate the final enhanced images of (a) and (b), respectively. The algorithm is as follows.

Image enhancement algorithm.

Input: A dental bitewing image I .

Output: An enhanced image with even teeth illumination and lower gum intensities.

Step1: Apply the proposed homomorphic filtering to I to remove uneven exposure.

- 1.1. Separate image I to illumination and reflection components using Eq. (2).
- 1.2. Retain the low-frequency illumination distribution by Gaussian low-pass filter using Eq. (3)
- 1.3. Take inverse transform and then anti-logarithm by Eq. (5) to obtain a reflection-suppressed image.
- 1.4. Dilate the reflection-suppressed image and divide it from the original image using Eq. (6).

Step2: Apply adaptive contrast stretching and adaptive morphological transformations to enlarge texture discrepancies between teeth and gums.

- 2.1. Measure the homogeneity of the filtered image resulted from *Step1* using Eqs. (9)–(14).
- 2.2. Calculate the degree of non-homogeneity using Eq. (15).

- 2.3. Establish the stretching function by determining the control points and slope using Eqs. (16)–(18).
- 2.4. Map the intensity of every pixel to a new value using Eq. (19).
- 2.5. Accentuate the cobweb-like texture in the gums using the adaptive morphological transformations in Eq. (20).

Step3: Apply the proposed homomorphic filtering to texture-image to lower the intensity of gums part.

- 3.1. Calculate the entropy $Q(x, y)$ and edge value $E(x, y)$ of the enhanced image I_E resulted from *Step2*.
- 3.2. Transform the enhanced image to texture feature space using

$$I_F(x, y) = \frac{Q(x, y) + E(x, y)}{2}. \quad (21)$$

- 3.3. Use I_F as the input image and perform *Step1* again to remove the high illumination portion and leave the part of gums that appear darker than the teeth.

2.2. Segmentation and contour extraction

After enhancement, the image is ready to be segmented. The segmentation method, which was adapted and modified from [18], is briefed as follows.

- *Teeth segmentation*: Segmentation starts with applying an initial thresholding to separate the enhanced image into teeth areas and background areas, where the initial threshold is estimated from an area around the edges of teeth [19]. A new threshold is then computed as the average of two mean gray values of the two areas. Thresholding is applied again if the new threshold is different from the previous one. This procedure is repeated until there is no change in the new threshold value. After iterative thresholding, the image is binary with teeth areas in white and background areas in black. At this point, the binary image is ready for isolation to each individual tooth.
- *Isolation*: Horizontal integral projection is first applied to separate the upper jaw from the lower jaw followed by vertical integral projection to each jaw [6]. The result is a set of blocks, usually called region of interest (ROI), each contains a tooth.
- *Pulp extraction*: The pulp is always located within the tooth and its intensity is lower. Thus, we apply the iterative thresholding again to extract the pulp from each ROI.
- *Contour extraction*: The shape boundary of each tooth and pulp are finally obtained by applying an edge operator to each ROI followed by equal points sampling and B-spline fitting [20] to obtain a smooth contour of each tooth and pulp. Note that spline fitting will not affect the dimensions of the tooth features that will be used for classification later; nevertheless, it can help us to view how well the extracted contours are.

3. Teeth classification

The goal of classification is to classify each tooth within a bitewing dental radiograph to molar or premolar. By observing many bitewing images, we conclude that relative length/width ratio of a tooth, relative length/width ratio of a pulp, and relative crown size are three features that can effectively classify molar teeth from premolar teeth.

3.1. ROI extension with angle adjustment

In many cases, teeth may appear skew due to shooting, injury, or poorly aligned when taking the radiograph, and some root areas may not appear as well. Therefore, the true length/width ratio of a tooth may not be available without angle adjustment of

that tooth. The ROI extension with angle adjustment is performed as follows.

Step1: Calculate the skew angle (θ_i) of each ROI_{*i*} of the upper/lower jaw, as

$$\theta_i = \begin{cases} T_i, & i = 1, \\ \frac{1}{2} \cdot (T_{i-1} + T_i), & 2 \leq i < n_j, \\ T_{i-1}, & i = n_j, \end{cases} \quad (22)$$

where T_i is the angle of the vertical boundary line, obtained during the isolation step of segmentation, and n_j is the maximum number of teeth in each jaw j .

Step2: For each ROI_{*i*} contained in the maxilla, pivot at the top-right or top-left corner of the sub-image containing the maxilla and rotate it $\text{abs}(\theta_i)$ degrees counter-clockwise if $\theta_i > 0$ or clockwise if $\theta_i < 0$.

Step3: For each ROI_{*i*} contained in the mandible, pivot at the top-left or top-right corner of the sub-image containing the mandible and rotate it $\text{abs}(\theta_i)$ degrees counter-clockwise if $\theta_i > 0$ or clockwise if $\theta_i < 0$.

Fig. 7 shows four extended ROIs after angle adjustment, in which (a) is a skewed image, (b) is the result of teeth segmentation and isolation with the angles of the three boundary lines of ROI's in maxilla and mandible being $(20^\circ, -4^\circ, -6^\circ)$ and $(20^\circ, 10^\circ, 10^\circ)$, respectively, (c) the extended ROI₁ in maxilla with $\theta_1 = 20^\circ$, (d) the extended ROI₂ in mandible with $\theta_2 = 15^\circ$, (e) the extended ROI₃ in maxilla with $\theta_3 = -5^\circ$, and (f) the extended ROI₄ in mandible with $\theta_4 = 10^\circ$.

3.2. Feature extraction

- **Relative length/width ratio (L/W):** The shape of a complete molar is relatively fatter than a skinny premolar. Similarly, the shape of pulps within molars is either wide-flat or square-like, which is significantly different from long-narrow pulps in premolars. We define length and width of ROI_{*i*} as:

$$\begin{cases} \text{length}_i(L_i) = \max(y_i) - \min(y_i), \\ \text{width}_i(W_i) = \max(x_i) - \min(x_i), \end{cases} \quad (23)$$

where (x_i, y_i) is the coordinate of any contour point in ROI_{*i*}. Thus, the relative length/width ratio of a tooth i in the upper/lower jaw j having n_j teeth is:

$$\frac{(L_i/W_i)_j}{(L/W)_j}, \quad i = 1 \dots n_j, j \in \{\text{maxilla}, \text{mandible}\},$$

where $(L/W)_j' = \frac{1}{n_j} \sum_{i=1 \dots n_j} (L_i/W_i)_j$. (24)

- **Relative crown size:** As mentioned in the introduction, the crown part of a tooth is defined as the upper portion of the tooth

bounded by the horizontal center line of the pulp. Observing the bitewing images available, we conclude that most of the crown parts of molars appeared significantly wider and bigger than those of premolars in the same image. Thus, we select relative crown size as another classification feature for discriminating molar teeth from premolar teeth. Since the complete crown part may not always appear in the image, we define the relative crown size as:

$$\frac{c_i}{c'}, \quad \text{where } c' = \sum_{i=1 \dots n} \frac{c_i}{n}, \quad (25)$$

and c_i is the width of ROI_{*i*} and n is the total number of teeth in the bitewing dental radiograph. Fig. 8 lists two sets of length/width ratio and crown width for premolar and molar tooth, respectively.

3.3. Support vector machine (SVM)

We use binary support vector machine (SVM) [21,22] to classify each tooth to molar or premolar. SVM is a popular classification and regression technique, which was originally derived from statistical learning theory and has shown promising empirical results in many practical applications. The basic idea of SVM is to transform data into a higher dimensional space and find the optimal hyperplane with maximal separation margin between classes.

We assume all data are linearly separable. That is, the hyperplane of our binary SVM has the form of $\mathbf{w} \cdot \mathbf{x} + b = 0$, where \mathbf{w} is the normal to the hyperplane and $b/\|\mathbf{w}\|$ is the perpendicular distance from the hyperplane to the origin. Fig. 9 is a scatter plot of the feature vectors (*relative teeth L/W , relative pulp L/W , relative crown size*)^T in our dataset.

A linear SVM works as follows. First, L data, (\mathbf{x}_i, y_i) ($i=1, \dots, L$), are randomly selected from the whole data set as the training set for finding the optimal \mathbf{w}^* and b^* such that the hyperplane $\mathbf{w}^* \cdot \mathbf{x} + b^* = 0$ is as far as possible from the closest members of both classes. That is, the training data (\mathbf{x}, y) s, named the support vectors, will fall on either side of the two planes $B_1 : \mathbf{w} \cdot \mathbf{x} + b = 1$





				
Teeth L/W	0.93	0.94	2.2	1.64
Pulp L/W	0.90	0.67	2.5	1.45
Crown Size (pixels)	185	196	104	138
	(a) Molar		(b) Premolar	

Fig. 8. Examples of the length/width ratio and crown size of molar and premolars.

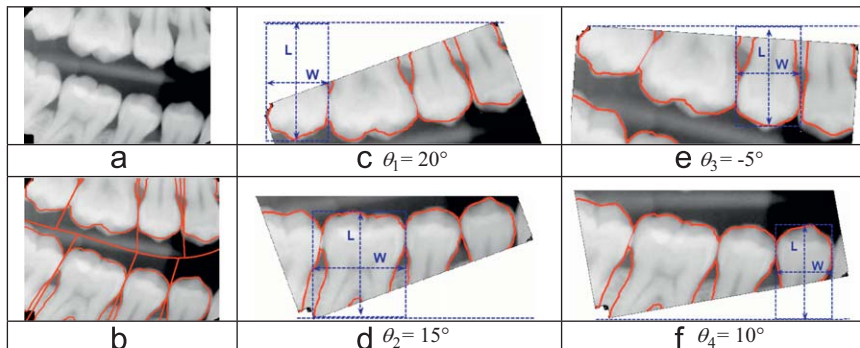


Fig. 7. Examples of ROI extension with angle adjustment.

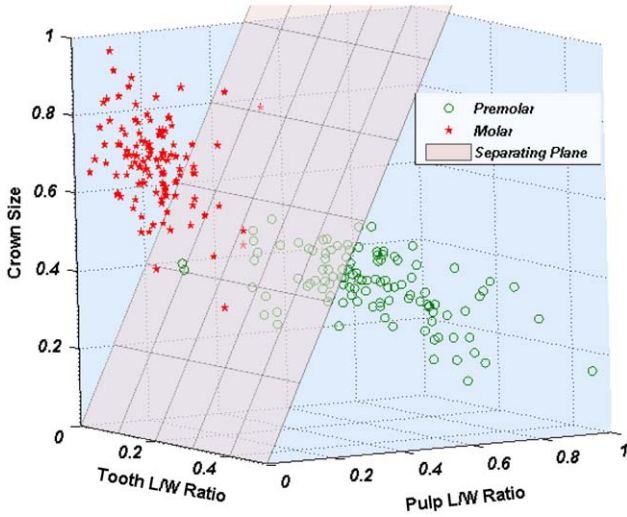


Fig. 9. The scatter plot of feature vectors.

and $B_2: \mathbf{w} \cdot \mathbf{x} + b = -1$. The hyperplane $\mathbf{w}^* \cdot \mathbf{x} + b^* = 0$ is thus called the decision boundary of this binary linear classifier.

Each training data is denoted by a tuple (\mathbf{x}_i, y_i) ($i=1,2,\dots,L$), where $\mathbf{x}_i = (x_{i1}, x_{i2}, \dots, x_{id})^T$ corresponds to the feature vector (relative teeth L/W, relative pulp L/W, relative crown size)^T, and $y_i \in \{1, -1\}$ denotes its class label, i.e., molar or premolar. Based on this binary linear SVM model, the optimal \mathbf{w}^* and b^* can be calculated as

$$\mathbf{w}^* = \sum_{i=1}^L \alpha_i y_i \mathbf{x}_i. \quad (26)$$

$$b^* = \frac{1}{N} \sum_{s \in S} (y_s - \sum_{m \in S} \alpha_m y_m \mathbf{x}_m \cdot \mathbf{x}_s) \quad (27)$$

where α is the Lagrange multiplier such that $\sum_{i=1}^L \alpha_i - (1/2) \alpha^T \mathbf{B} \alpha$ is maximized, subject to the constraints $\alpha_i \geq 0 \forall i$ and $\sum_{i=1}^L \alpha_i y_i = 0$, \mathbf{B} is a matrix with $B_{ij} = y_i y_j \mathbf{x}_i \cdot \mathbf{x}_j$, and S is the set of support vectors whose $\alpha_i > 0$.

After constructing the decision hyperplane, each testing data \mathbf{x}' is assigned to one of the two classes by evaluating $y' = \text{sgn}(\mathbf{w}^* \cdot \mathbf{x}' + b^*)$, where $\text{sgn}(\cdot)$ is the sign function. That is, \mathbf{x}' belongs to class molar if $y' > 0$; otherwise, it belongs to class premolar.

4. Teeth numbering

Teeth numbering assigns each molar or premolar in both mandible and maxilla to a unique number according to the universal teeth numbering system. Our numbering method firstly formats each of the maxilla and mandible sequences to be a sequence comprising 'P', 'M', or '-', using both the classified result and the distances between each pair of the neighboring teeth. The formatted sequences are then compared with two standard patterns for a best matching segment using a simplified sequence alignment technique commonly used in bioinformatics. Finally, the specific number is assigned to each tooth based on the universal teeth numbering system.

4.1. Teeth standard patterns

Bitewing radiographs are taken either from the left or the right side of jaws. Each radiograph may contain one to three molars and

Table 1

Two standard teeth patterns and numbers of bitewing radiographs.

Type	Pattern-1						Pattern-2					
	M	M	M	P	P	P*	P*	P	P	M	M	M
Maxilla	1	2	3	4	5	6	11	12	13	14	15	16
Mandible	32	31	30	29	28	27	22	21	20	19	18	17

Note: P stands for premolar and M stands for molar. P* is named cuspid (canine) in the universal teeth numbering system.

premolars, respectively in both maxilla and mandible. Thus, the maximum number of teeth in each jaw is six. As shown in Fig. 2, (a) contains three premolars and one molar in both maxilla and mandible, respectively, (b) contains three premolars and one molar, and two premolars and two molar in both maxilla and mandible, respectively, (c) contains two molars and two premolars in both maxilla and mandible, respectively, and (d) contains three molars and two premolars in maxilla, and three molars and one premolar in mandible. For being able to fit the proposed numbering algorithm in all possible bitewing radiographs, we define the standard teeth patterns and their teeth numbers from left to right as M(1)M(2)M(3)P(4)P(5)P(6) for maxilla and M(32)M(31)M(30)P(29)P(28)P(27) for mandible, respectively for left jaw images and P(11)P(12)P(13)M(14)M(15)M(16) for maxilla and P(22)P(21)P(20)M(19)M(18)M(17) for mandible, respectively, for right jaw images, as listed in Table 1. Note that we name the canine teeth as the third premolars for ease of numbering.

4.2. Teeth sequence formation

After classification, each tooth in maxilla or mandible is labeled as either molar 'M' or premolar 'P'. Before aligning to the standard pattern, we need to first aggregate the teeth in each maxilla and mandible to be a sequence of ' $x_1 x_2 \dots x_m$ ', where $x_i = \text{'M'}$, ' 'P' ', or ' $\text{'-'} (missing tooth)$ ', $m \leq 6$. The sequence formation procedure is as follows:

Step1: Make a sequence by concatenating each tooth label from left to right.

Step2: Insert t notation '-'s to the corresponding positions of the sequence if t missing teeth are identified, where

$$t = \arg \min_{t=1 \dots n} \left\{ \left(\frac{d_i}{(1/2) \cdot c_i + c_{i+1} \cdot t - 1/2} \right) > 1 \right\}, \quad 1 \leq i \leq m-1. \quad (28)$$

and $n=m-1$ is the maximum number of missing teeth needed to be handled, c_i and c_{i+1} are the two neighboring relative crown sizes associated with the corresponding valley of the integral projection curve.

2.1: Calculate the distance d_i ($1 \leq i \leq m-1$), of the valleys in the integral projection curve along the y-axis taken during the teeth isolation.

2.2: For each d_i , start with $t=1$ and identify t teeth missing at this position if $d_i > ((1/2) \cdot (c_i + c_{i+1}) \cdot (t - 1/2))$; otherwise, bump t by one and repeat the condition checking.

2.3: Insert t notation '-'s to the corresponding position into the sequence if t missing teeth are identified.

Fig. 10 gives a simple example of teeth-sequence formation. As shown in 10(b), we can see that the distance $d_1 < (c_1 + c_2)/4$ (no missing teeth), and $d_2 > (c_2 + c_3)/4$ (missing one tooth). Therefore, the final teeth sequence of mandible is 'PP-M'.

4.3. Teeth alignment and numbering algorithm

A bitewing radiograph could be either taken from the left or the right jaw. Thus, both standard patterns and their corresponding numbers, as listed in Table 1, are required for the numbering algorithm.

$$O_{ij} = \begin{cases} O_{i-1,j-1} + 1, & \text{if } t_i \text{ and } p_j \text{ are match.} \\ \max\{O_{i-k,j-k} - \frac{1}{3} \cdot k, 0\}, & \text{if } t_i \text{ and } p_j \text{ are } k\text{-associated, } k = 1, \dots, \min(i, j). \end{cases} \quad (29)$$

Teeth numbering algorithm.

Input: Two teeth sequences, two standard teeth patterns and their respective tooth numbers.

Output: Two sequences of teeth numbers.

Step1: Identify which standard pattern should be used for teeth alignment.

- 1.1 Calculate four similarity matrices O_{max_1} , O_{max_2} , O_{man_1} , and O_{man_2} between each of the two teeth sequences (maxilla and mandible) and the two standard patterns (Pattern-1 and Pattern-2) using our simplified version of Smith–Waterman algorithm [23], as we only consider contiguous subsequences (segments) containing no internal deletions or insertions. Let the teeth sequence be $T = t_1 t_2 \dots t_m$ and the pattern sequence

be $P = p_1 p_2 \dots p_n$, $m \leq n$, respectively. Define t_i and p_j be (i) match if $t_i = p_j$, (ii) 1-associated if $t_i = '-'$, and (iii) k -associated, $1 \leq k \leq \min(i, j)$ if $t_{i-k} = p_{j-k}$. Then the similarity matrix $O = \{O_{ij}\}$, the degree of similarity between pairs of segments T_i and P_j ending at t_i and p_j , respectively, can be calculated as

Note that constant $1/3$ is adapted from Smith–Waterman algorithm.

- 1.2 Set the similarity score of each maxilla and mandible teeth sequence against each standard pattern, denoted S_{max_i} , S_{man_i} , $i = 1, 2$, to be the maximum value of each corresponding similarity matrix. Compute the total similarity score S_i of the image against each standard pattern- i by $S_i = S_{max_i} + S_{man_i}$, $i = 1, 2$.
- 1.3 Select the standard pattern to which the total similarity score of the teeth sequence is higher as the pattern template for alignment. That is, select 'Pattern-1' if $S_1 \geq S_2$; otherwise, select 'Pattern-2'.

Step2: Align each teeth sequence against the chosen standard pattern, respectively.

- 2.1 Select the teeth sequence whose similarity score to the pattern template is higher as the first sequence to be aligned. That is, align the maxilla sequence first if $S_{max} > S_{man}$ or vice versa. When the two sequences have the same similarity to the pattern template, align each sequence against the pattern template individually using only steps 2.2 and 2.3.
- 2.2 Locate the maximum element from the last row of the similarity matrix at O_{kl} and find the longest local matching subsequence (LLMS) as $p_{l-k+1} p_{l-k+2} \dots p_{l-1} p_l$ where k is the length of the teeth sequence under alignment.
- 2.3 Replace t_i with p_{l-k+i} , $1 \leq i \leq k$ if $t_i \neq p_{l-k+i}$ and superimpose $p_{l-k+1} p_{l-k+2} \dots p_{l-1} p_l$ onto the pattern template $p_1 p_2 \dots p_n$.
- 2.4 Align the other sequence $t_1 t_2 \dots t_h$ with the LLMS $p_{l-k+1} p_{l-k+2} \dots p_{l-1} p_l$, by one of the following actions. (a) $h = k$: Align directly with $p_{l-k+1} p_{l-k+2} \dots p_{l-1} p_l$. (b) $h < k$: Find the LLMS between $t_1 t_2 \dots t_h$ and $p_{l-k+1} p_{l-k+2} \dots p_{l-1} p_l$ by locating the maximum element from the last row of the similarity matrix O_{hk} and finding the LLMS as $p_{k-h+1} p_{k-h+2} \dots p_{k-1} p_k$. (c) $h > k$: Find the LLMS between $t_1 t_2 \dots t_h$ and $p_{l-k+1} p_{l-k+2} \dots p_{l-1} p_l$ by locating the maximum element from the similarity matrix O_{hk} at (a, b) , $1 \leq a \leq h$, $1 \leq b \leq k$, and finding the LLMS as $p_{b-a+1} p_{b-a+2} \dots p_{b-1} p_b$.
- 2.5 Replace t_i with the aligned element p_j in the matched LLMS if $t_i \neq p_j$, and superimpose the corrected $t_1 t_2 \dots t_h$ onto the standard pattern at the aligned location.

Step3: Number each tooth based on the aligned standard pattern.

Fig. 11 depicts the general flow diagram of this numbering algorithm.

4.4. Examples

A radiograph with 'PPPM' (11, 12, 13, 14) in maxilla and 'PPM' (21, 20, 19) in mandible has been classified to 'PPPM' and 'PMM' for maxilla and mandible, respectively.

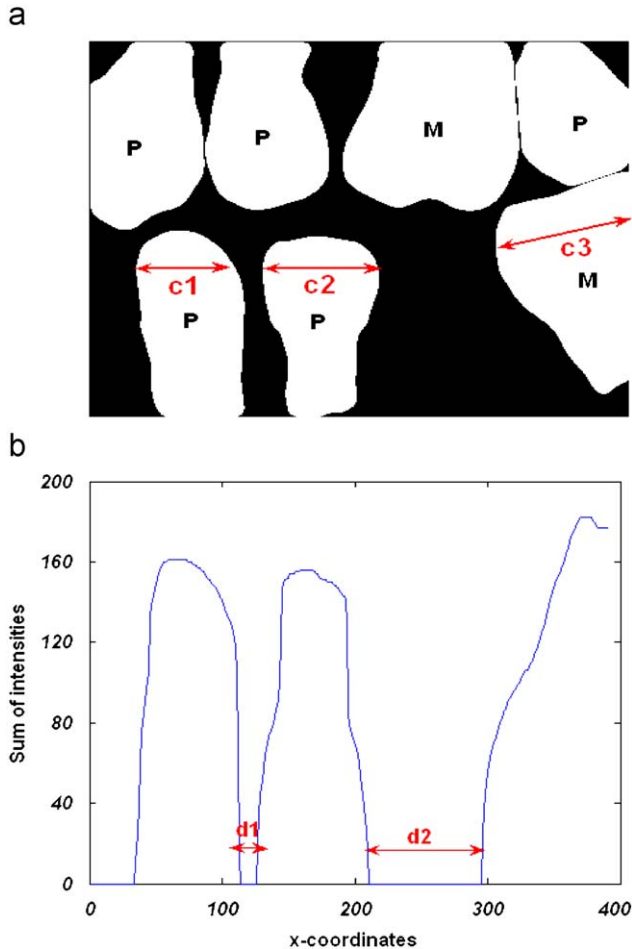


Fig. 10. An example of teeth sequence formation: (a) one missing tooth in the lower jaw, (b) the vertical integral projection of the lower jaw.

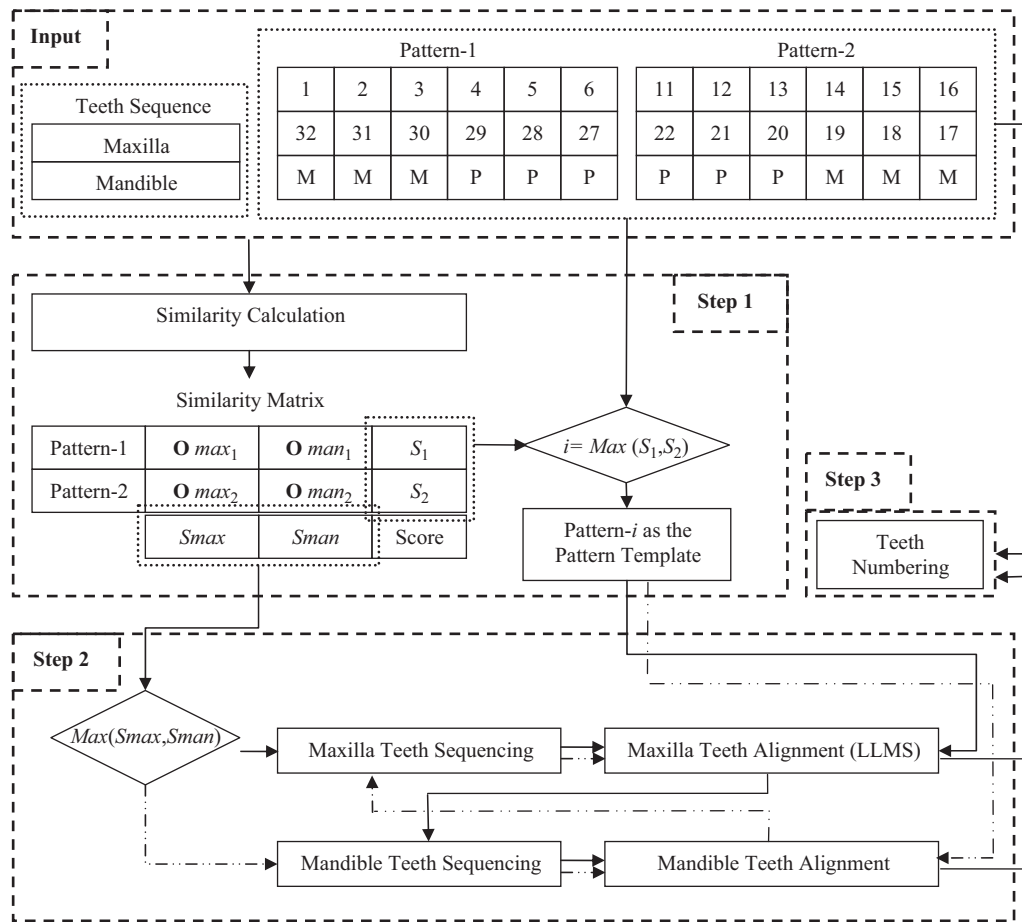


Fig. 11. The flow chart of our numbering algorithm.

Step1:

1.1: Calculate the similarity matrices \mathbf{Omax}_1 , \mathbf{Omax}_2 , \mathbf{Oman}_1 , \mathbf{Oman}_2 as

\mathbf{Omax}_1	M	M	M	P	P	P	\mathbf{Omax}_2	P	P	P	M	M	M
P	0	0	0	1	1	1	P	1	1	1	0	0	0
P	0	0	0	1	2	2	P	1	2	2	0.7	0	0
P	0	0	0	1	2	3	P	1	2	3	1.7	0.3	0
M	1	1	1	0	0.7	1.7	M	0	0.7	1.7	4	2.7	1.3

\mathbf{Oman}_1	M	M	M	P	P	P	\mathbf{Oman}_2	P	P	P	M	M	M
P	0	0	0	1	1	1	P	1	1	1	0	0	0
M	1	1	1	0	0.7	0.7	M	0	0	0.7	2	1	1
M	1	2	2	0.7	0	0.3	M	0	0	0	1.7	3	2

1.2: Obtain the two similarity score S_i , $i=1$ (maxilla), 2 (mandible) as

	MMMPPP	PPPM
Maxilla (PPPM)	$Smax_1=3$	$Smax_2=4$
Mandible (PMM)	$Sman_1=2$	$Sman_2=3$
Score	$S_1=5$	$S_2=7$

1.3: Select 'Pattern-2' 'PPPM' as the standard pattern template, as $S_2=7 > 5=S_1$.

Step2:

2.1: Align maxilla sequence 'PPPM' first as it has higher score, i.e., $Smax=4 > 3=Sman$.

2.2: The LLMS of maxilla sequence is 'PPPM', as $\mathbf{Omax}_2(4,4)=4$, the maximum element of the last row in \mathbf{Omax}_2 .

2.3: Superimpose 'PPPM' onto the pattern template 'PPPM'.

2.4: The LLMS of mandible sequence 'PMM' and 'PPPM' is 'PMM', as $\mathbf{Oman}(3,4)=1.7$, the maximum element of the last row in \mathbf{Oman} ($h < k$).

\mathbf{Oman}	P	P	P	M
P	1	1	1	0
M	0	0.7	0.7	2
M	0	0	0.3	1.7

2.5: Replace 'PMM' with 'PPM' and the superimposed alignment is 'PPPM'.

Step3:

The teeth numbers of maxilla and mandible are (11,12,13,14) and (21,20,19), respectively, as maxilla sequence 'PPPM' lines up against 'PPPM' and mandible sequence 'PMM' lines up against 'PPPM'.

5. Experimental results and comparisons

We perform two experiments for our proposed system and compare the experimental results with those of the method in

[12]. The test environment is AMD Athlon 64 X2 Dual with CPU 3800 and 2G RAM running in Window XP platform. The software package used is MATLAB and LIBSVM in [22].

5.1. Segmentation and classification results

We use 47 bitewing images taken from either the left or the right jaw with 369 teeth in total in this experiment. After segmentation, we successfully isolate 348 teeth in total, in which 87 and 91 teeth are molars in maxilla and mandible, respectively, and 92 and 78 teeth are premolars in maxilla and mandible, respectively. We select nine segmented images containing 17 and 19 molars, and 16 and 13 premolars, in maxilla and mandible, respectively as the training set for SVM, and use the rests as the testing set. The experimental results indicate that 65 out of the 70 (92.9%) molars in maxilla, 69 out of the 72 (95.8%) molars in Mandible, 75 out of the 76 (98.7%) premolars in maxilla, and 60 out of the 65 (92.3%) premolars are classified correctly. In other words, the system achieves an overall classification accuracy rate of 95.1%. Fig. 12 shows eight segmented and classified dental images of the testing set; whereas the column “pre-(5)” of our method” in Table 2 summarizes the classification results.

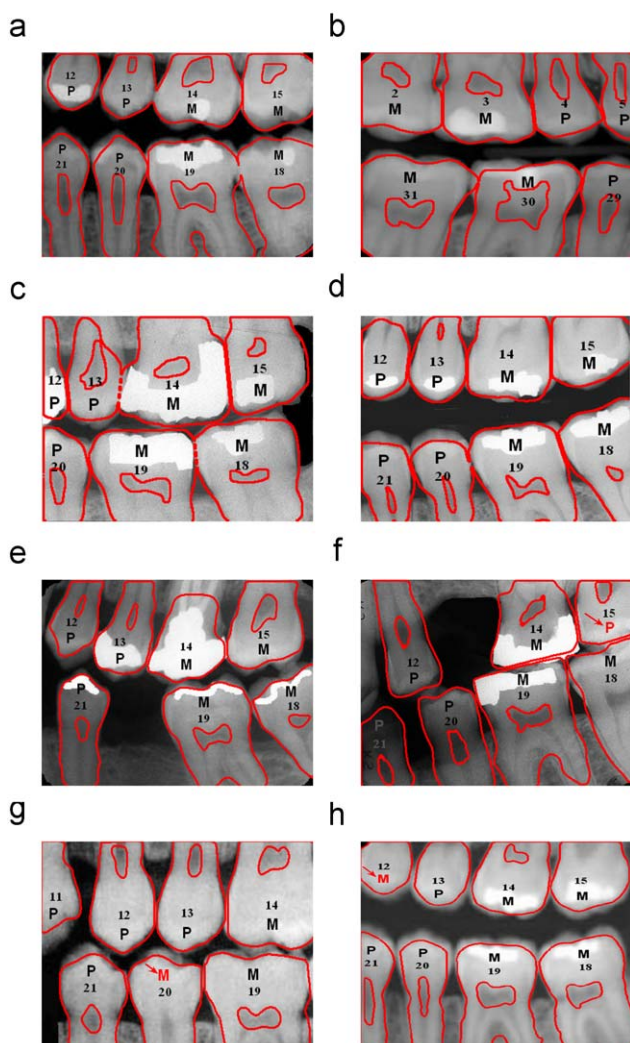


Fig. 12. Examples of the segmentation and classification results: (a)–(e) correct classification and numbering, (f)–(h) misclassification but correct numbering.

Table 2

Comparison of classification accuracy (in %).

Teeth	Our method		Method 1 by Mahoor [12]		Method 2 by Mahoor [12]	
	pre-(5)	final-(6)	pre-	final-	pre-	final-
(1)	95.8	95.8	(7) 95.5/95.5	95.5/95.5	89.7/89.3	91.8/91.4
(2)	92.3	100	86.4/81.5	86.4/84.2	82.7/78.7	91.4/85.1
(3)	92.9	100	83.7/86.4	93.7/95.5	91.4/86.4	93.7/91.4
(4)	98.7	100	86.4/72.0	92.0/90.0	72.0/80.0	82.0/94.2

- (1) Molars in mandible.
- (2) Premolars in mandible.
- (3) Molars in maxilla.
- (4) Premolars in maxilla.
- (5) Pre-classification: without teeth numbering.
- (6) Final classification: with teeth numbering.
- (7) Classification result by using: complex signature/centroid distance.

Table 3

Numbering accuracy.

	# of images	Accuracy (%)	# of teeth	Accuracy (%)
Accurately classified	35	97.1	255	98.8
Misclassified	12	91.7	93	95.7
Total	47	95.7	348	98.0

5.2. Numbering results

We use the same 47 classified bitewing images to test effectiveness of our numbering algorithm, where 35 images are 100% accurately classified and 12 images have one or two misclassified teeth. The experimental results indicate that all teeth in 34 out of the 35 (97.1%) accurately classified images and 11 out of the 12 (91.7%) partially misclassified images are correctly numbered. In terms of number of teeth, 252 out of 255 (98.8%) accurately classified teeth and 89 out of 93 (95.7%) misclassified teeth are correctly numbered. In other words, our numbering method achieves a total accuracy rate of 95.7% (45/47) and 98.0% (341/348), respectively in terms of number of images and number of teeth, respectively. In addition, applying the teeth sequence alignment steps of the numbering method can also correct some of the misclassification results, as shown with ‘↘’ in Figs. 12(f)–(h). The differences between the values in column “pre-(5)” and “final-(6)” of our method in Table 2 demonstrate the improvement of classification; whereas Table 3 summarizes the numbering accuracy of the test.

5.3. Comparisons

We claim that our method outperform the method in [12] based on the successful results of applying our teeth classification and numbering system on four bitewing radiographs that were reported in [12] either misclassified or mis-numbered, as shown in Figs. 13(a)–(d). Note that all four images are taken from the left side of jaws, so the correct teeth pattern should be ‘PPMM’. Figs. 13(a2)–(d2) demonstrate that our method correctly classify the two images that were reported misclassified, as shown in Figs. 13(a1) and (b1), and correctly number the two images that were reported incorrectly numbered, as shown in Figs. 13(c1) and (d1). Table 2 compares the classification accuracy rates between our method and all their methods, though the data set used in experiments may not be completely identical. Observing the

classification results, we can see that all their methods cannot simultaneously classify molars and premolars with high accuracy, even after applying spatial relation adjustment, as listed in columns final. Our accuracy rates of 94.4% (134/142) for molars and 95.7% (135/141) for premolars indicate that our method can simultaneously classify molars and premolars in high accuracy. The rates are improved further to 97.9% (139/142) for molars and 100% (141/141) for premolars if we apply teeth numbering for final classification.

5.4. Unsolved or failure cases

Although as demonstrated in Fig. 13, our numbering method can correct misclassification in cases of (a) both maxilla and mandible teeth sequence patterns are the same, and (b) one sequence is the sub-pattern of the other. However, two situations still result in errors.

The first one occurs when two classified teeth sequences, in that one is misclassified, have the same similarity score and each can find a completely matched segment in the standard pattern. Since we do not know which matched segment is correct so that we cannot pick one as the correct segment for the other to align with. In such cases, the alignment algorithm cannot achieve classification-correction. Fig. 14(a) shows an example of this situation, where the accurately classified maxilla sequence 'PPPM' is completely matched with the segment 'PPPM' in the standard pattern 'PPPMMM', and the misclassified mandible sequence 'PMMM' is also completely matched with the segment 'PMMM' within the standard pattern 'PPPMMM'. Therefore, the misclassified sequence is aligned with the wrong segment and still results in error.

The other situation occurs when the teeth arrangement of both jaws is not consistent. Fig. 14(b) is one of such example, where the mandible sequence 'MMM' is not a segment of the maxilla sequence 'MMPP'. Since 'MMPP' has higher similarity score that it

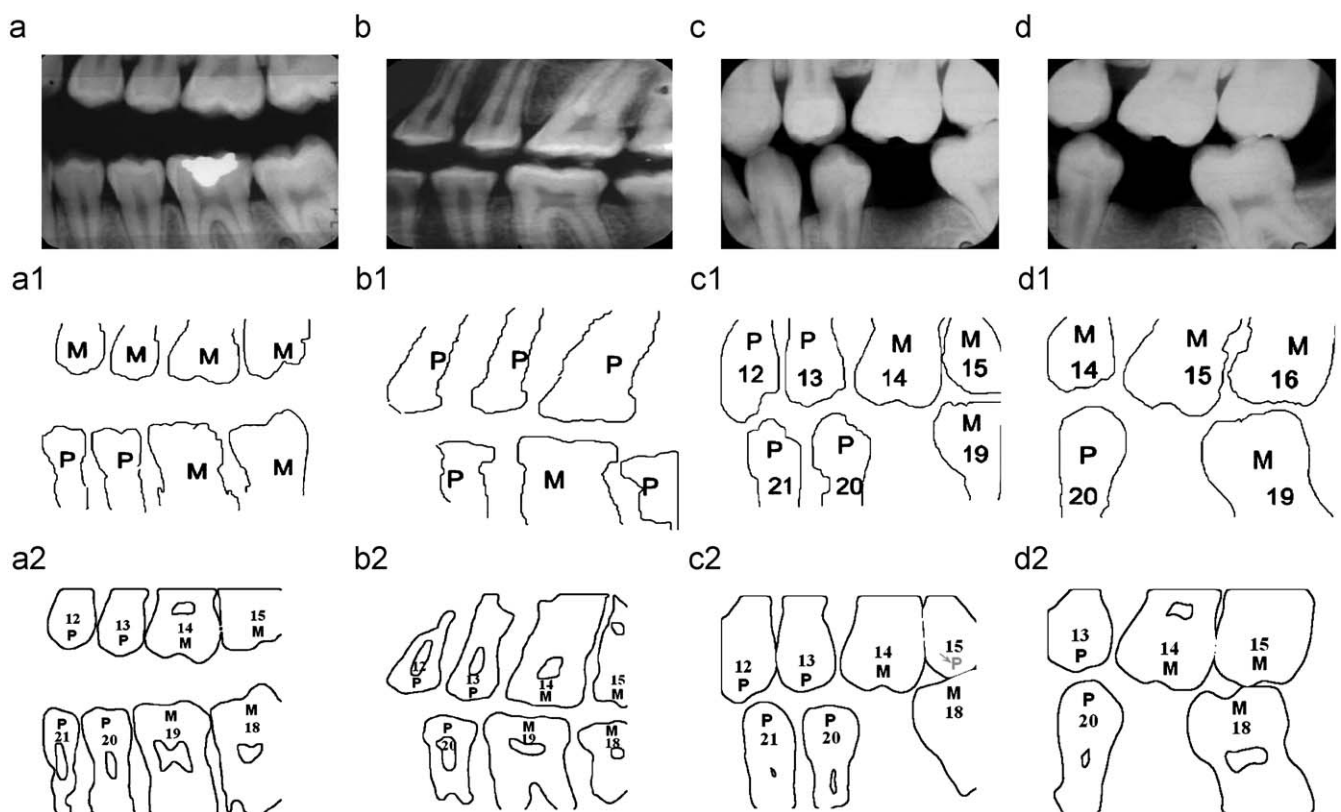


Fig. 13. Comparison of the misclassification and incorrect numbering results of method in [12]. (a)–(d) original images, (a1),(b1) misclassified in [12], (c1),(d1) incorrectly numbered in [12], (a2),(b2) accurately classified by our method, (c2),(d2) accurately numbered by our method.

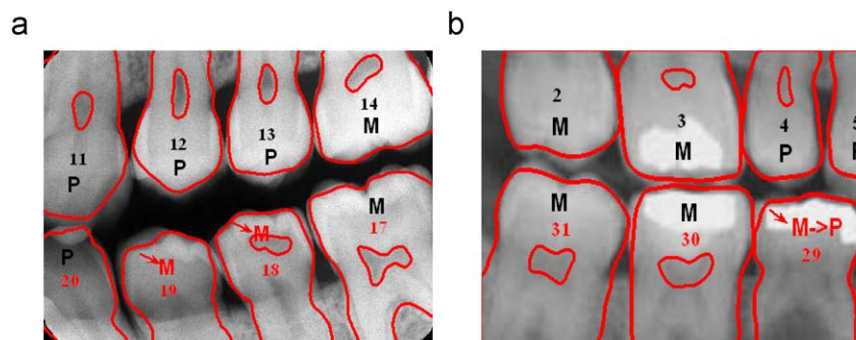


Fig. 14. Two failure cases of our numbering method.

will be used as the alignment segment for the mandible sequence 'MMM'. As a result, 'MMM', even though it is originally a correct classification sequence, will be 'wrongly aligned and corrected' to 'MMP'.

We also notice that some of the extracted teeth contours in the segmentation results still do not cover the entire teeth and some pulps have not been extracted, even though the intensity differences between teeth and gums and between teeth and pulps are visible in the enhanced images. This suggests that the adapted simple iterative thresholding should be further improved for better segmentation results.

6. Conclusions

Teeth segmentation, classification, and numbering for dental radiographs are important but still challenging for automatically and accurately identifying long-missing people or victims in mass disasters. In this paper, we presented a dental classification and numbering system, including an image enhancement method for improving segmentation teeth from other parts, an effective way of extracting robust features for increasing the accuracy of classification, and a simplified version of a sequence alignment algorithm commonly used in bioinformatics for teeth alignment with the universal teeth numbering system. We showed that (i) applying the proposed homomorphic filtering and homogeneity-based contrast stretching techniques can indeed enhance images to appear with even illumination and better contrast for iterative thresholding, (ii) using three features that include both contour and region information and adjusting each ROI orientation then extending the ROI to include the missing root area is effective for classification, (iii) our teeth alignment and numbering algorithm further improves the classification accuracy, (iv) our system outperforms a presented method in both classification accuracy and capability of accurately classifying difficult images. Despite of good results demonstrated, classifying poor images, such as only 3 or 4 teeth left, teeth arrangement of both upper and lower jaws is not consistent, or teeth in upper and lower jaws overlapped each other, is still a big challenge.

Acknowledgment

This research was supported by the National Science Council of ROC under Grants NSC-97-2221-E-126-008 and NSC 96-2628-E-005-084-MY3.

References

- [1] M. Abdel-Mottaleb, O. Nomir, D.E. Nassar, G. Fahmy, H.H. Ammar, Challenges of developing an automated dental identification system, *IEEE Int. Mid-west Symp. Circuits Syst.* 1 (2003) 411–414.
- [2] G. Fahmy, D. Nassar, E. Haj-Said, H. Chen, O. Nomir, J. Zhou, R. Howell, H. Ammar, M. Abdel-Mottaleb, A. Jain, Toward an automated dental identification system (ADIS), *J. Electron. Imaging* 14 (2005) 1–13.
- [3] American Dental Association, *Current Dental Terminology*, third ed. (CDT-3), 1999.
- [4] A.K. Jain, H. Chen, Matching of dental X-ray images for human identification, *Pattern Recognition* 37 (2004) 1519–1532.
- [5] J. Zhou, M. Abdel-Mottaleb, A content-based system for human identification based on bitewing dental X-ray images, *Pattern Recognition* 38 (2005) 2132–2142.
- [6] O. Nomir, M. Abdel-Mottaleb, A system for human identification from X-ray dental radiographs, *Pattern Recognition* 38 (2005) 1295–1305.
- [7] F. Keshkar, W. Gueaieb, Segmentation of dental radiographs using a swarm intelligence approach, *Can. Conf. on Electr. Comp. Eng.* (2006) 328–331.
- [8] E.H. Said, D.E.M. Nassar, G. Fahmy, H.H. Ammar, Teeth segmentation in digitized dental X-ray films using mathematical morphology, *IEEE Trans. Inf. Forensic Secur.* 1 (2006) 178–189.
- [9] S. Li, T. Fevens, A. Krzyzak, C. Jin, S. Li, Semi-automatic computer aided lesion detection in dental X-rays using variational level set, *Pattern Recognition* 40 (2007) 2861–2873.
- [10] Y.H. Lai, P.L. Lin, Effective segmentation for dental X-ray images using texture-based fuzzy inference system, *Adv. Concepts Intell. Vision Syst. LNCS* 5259 (2008) 936–947.
- [11] S. Tabbone, L. Wendling, J.-P. Salmon, A new shape descriptor defined on the Radon transform, *Comput. Vision Image Underst.* 102 (2006) 42–51.
- [12] M.H. Mahoor, M. Abdel-Mottaleb, Classification and numbering of teeth in dental bitewing images, *Pattern Recognition* 38 (2005) 577–586.
- [13] A.K. Jain, H. Chen, Registration of dental atlas to radiographs for human identification, *Proc. of SPIE Conf. on Biom. Technol. Hum. Identification* 5779 (2005) 292–298.
- [14] T. Acharya, A.K. Ray, *Image Processing: Principles and Applications*, Wiley-Interscience, 2005.
- [15] L.G. Shapiro, G.C. Stockman, *Computer Vision*, Prentice Hall, 2001.
- [16] H.D. Cheng, M. Xue, X.J. Shi, Contrast enhancement based on a novel homogeneity measurement, *Pattern Recognition* 36 (2003) 2687–2697.
- [17] A. Moragas, M. Garcia-Bonafe, I. de Torres, M. Sans, Textural analysis of lymphoid cells in serous effusions. A mathematical morphologic approach, *Anal. Quant. Cytol. Histol.* 15 (1993) 165–170.
- [18] O. Nomir, M. Abdel-Mottaleb, Fusion of matching algorithms for human identification using dental X-ray radiographs, *IEEE Trans. Inf. Forensic Secur.* 3 (2008) 223–233.
- [19] R.C. Gonzalez, R.E. Woods, *Digital Image Processing*, second ed., Prentice Hall, 2002.
- [20] C. de Boor, B-Spline basics, in: L.A. Piegl (Ed.), *Fundamental Developments of Computer-Aided Geometric Modeling*, Academic Press, New York, 1993, pp. 27–49.
- [21] C. Cortes, V. Vapnik, Support-vector network, *Mach. Learn.* 20 (1995) 273–297.
- [22] C.C. Chang, C.J. Lin, LIBSVM: A library for support vector machines, 2001, software available at <<http://www.csie.ntu.edu.tw/~cjlin/libsvm>>.
- [23] T.F. Smith, M.S. Waterman, Identification of common molecular subsequences, *J. Mol. Biol.* 147 (1981) 195–197.

About the Author—PHEN-LAN LIN received her BS degree in Engineering Science from Taiwan National Cheng-Kung University in 1973, both MSEE and Ph.D. degrees in Electrical Engineering from Southern Methodist University, Dallas, Texas in 1992, and 1994, respectively. She is a professor in the Department of Computer Science and Information Engineering, Providence University since 2004, and had been a professor and an associate professor in the Department of Computer Science and Information Management in 1995–2003, as well as the Director of Computer and Communication Center in the university in 2002–2008. Prior teaching, Dr. Lin was with Texas Instruments in Dallas, Texas as a member of technical staff, lead engineer, and project manager from 1978 to 1992, respectively. Her current research interests include information security and privacy (including multimedia and network security), medical imaging, and automatic visual inspection.

About the Author—YAN-HAO LAI received his BS degree in Information Management from South Taiwan University in 2003. He is currently a Ph.D. student in the Department of Computer Science and Engineering of National Chung-Hsing University. His research interests include computer vision and information security.

About the Author—PO-WHEI HUANG received his BS degree in applied mathematics from National Chung-Hsing University in 1973, the MS degree in mathematics from Texas Tech University in 1978, and the Ph.D. degree in computer science from Southern Methodist University in 1989. He was with Texas Instruments in Dallas as a member of technical staff, project manager, and software development manager from 1978 to 1990. He was the department chairman and has been a professor in the Department of Computer Science and Engineering at National Chung-Hsing University. From September 2002 to October 2004, he served as the vice president of National Huwei University of Science and Technology located in Yunlin County of Taiwan. From October 2004 to January 2006, he was appointed as the Secretary General of National Chung-Hsing University. Since February 2006, he has been the dean of College of Science at National Chung-Hsing University. His research interests include image database, computer vision, pattern recognition, and artificial intelligence.